Brain & Development 41 (2019) 195–200

BRAIN & DEVELOPMENT
Official Journal of the Japanese Society of Child Neurology

www.elsevier.com/locate/braindev

Case Report

Aggregate formation analysis of GFAP^{R416W} found in one case of Alexander disease

Janyerkye Tulyeu [a,1], Moe Tamaura [b,1], Eriko Jimbo [a], Hiroko Shimbo [b], Kyoko Takano [d], Mizue Iai [b], Sumimasa Yamashita [b], Tomohide Goto [b], Noriko Aida [c], Etsuro Tokuhiro [e], Takanori Yamagata [a], Hitoshi Osaka [a,*]

[a] *Deptartment of Pediatrics, Jichi Medical School, 3311-1 Yakushiji, Shimotsuke-shi, Tochigi 329-0498, Japan*
[b] *Division of Neurology, Kanagawa Children's Medical Center, Yokohama, Japan*
[c] *Radiology, Kanagawa Children's Medical Center, Yokohama, Japan*
[d] *Department of Medical Genetics, Shinshu University School of Medicine, Matsumoto, Japan*
[e] *Department of Pediatrics, Odawara Municipal Hospital, Kanagawa, Japan*

Received 10 May 2018; received in revised form 9 August 2018; accepted 27 August 2018

Abstract

Alexander disease (AxD) is a neurodegenerative disease in astrocytes caused by a mutation in the gene encoding glial fibrillary acidic protein, *GFAP*. We herein present the case of a 12-year-old girl who showed intermittent exotropia at 3 years of age and central precocious puberty at 7 years of age. The periventricular and medulla oblongata showed high signal intensity on T2-weighted magnetic resonance imaging. The patient was diagnosed with AxD after direct sequencing revealing a *de novo* recurrent mutation, c.1246C>T (p.R416W) in *GFAP*. The transient expression of GFAP^{R416W} in cells resulted in the significant formation of aggregates, which recapitulated the hallmark of AxD. We firstly utilized In Cell analyzer to prove the tendency of aggregate formation by mutants of GFAP.

Keywords: Alexander disease (AxD); Glial fibrillary acidic protein (GFAP); Aggregation; Precocious puberty

1. Introduction

Alexander disease (MIM 203450; AxD) is a dominantly inherited devastating degenerative leukoencephalopathy caused by mutations in *Glial Fibrillary Acidic Protein* (*GFAP*) [1,2] GFAP is an intermediate filament III protein that is expressed in astrocytes, non-myelinating Schwann cells, and enteric glial cells [3].

The pathological feature of AxD include cytosolic aggregates, Rosenthal fibers (RFs), in astrocytes. RFs are composed of misfolded GFAP proteins and chaperone proteins such as αB-crystallin and heat shock protein 27 (HSP-27). Similar type of aggregation were also found in the iPSC-derived astrocytes from an AxD patient [4]. AxD is classified into the early-onset severe type and the later-onset mild type [5]. The infantile type of the former classification corresponds to the severe type, whereas both the juvenile and adult types correspond to the mild type [6]. The clinical symptoms of severe AxD include motor and mental retardation, bulbar dysfunction, seizures, microcephalus, and

* Corresponding author.
E-mail address: hosaka@jichi.ac.jp (H. Osaka).
[1] Equally contribute.

https://doi.org/10.1016/j.braindev.2018.08.009

typically early death in the first decade of life [1]. Patients with mild type AxD display muscle weakness, spasticity and ataxia in the second or third decades of life [5]. However, the genotype and phenotype correlations are not fully understood.

We herein report the case of a patient with the mild type AxD with c.1246C>T (p.R416W) in *GFAP* [7–9]. The patient presented precocious puberty and subsequent weight loss. We quantitatively compared the aggregate formation of this mutation with the mild type of c.772C>T (p.Arg258Cys) and the severe type of c.715C>T (p.Arg239Cys) using In Cell analyzer.

2. Patient

The patient was the first child of non-consanguineous and healthy Japanese parents. Her prenatal and perinatal periods were not remarkable. Her developmental milestones were normal. Intermittent exotropia was noticed at 3 years of age. At 7 years of age, her breasts enlarged and the periventricular area showed a high intensity on T2-weighted brain MRI. At 8 years of age, her serum levels of LH, FSH, and E2 (hormones) were elevated and her bone age was accelerated. She was diagnosed with central precocious puberty and treated with GnRH analog and anabolic steroids at 11 years of age.

Soon after the initiation of therapy, she presented with weight loss without feeding problems and was brought to the hospital. She then suffered several attacks that last few second in which she experienced a loss of consciousness in a month. Electroencephalogram was unremarkable. At 12 years of age, she presented increasing hiccups and belching with bouts of vomiting and admitted to our hospital. A physical examination revealed the following: body weight, 26.1 kg (−2.2SD), height, 137 cm (−2.6 SD); head circumference, 53 cm (50th percentile); and BMI, 13.9 kg/m^2. Her breasts were Tanner stage II, and she had axillary hair. A neurological examination revealed dysphagia, weak grip strength, and knee reflex accentuation, and scoliosis was found. The other general physical examination results were unremarkable. Serum laboratory examinations revealed unremarkable. A cerebrospinal fluid analysis showed an increase in lactic acid 22.7 mg/dL and pyruvic acid 1.29 mg/dL. Brain magnetic resonance imaging (MRI) revealed an area of high signal intensity along both lateral ventricles on T1-weighted imaging (Fig. 1A) with contrast enhancement, and a periventricular rim of decreased signal intensity surrounded by an area of high signal intensity on T2-weighted imaging (Fig. 1B). A high signal intensity was observed from the lower medulla oblongata to the upper cervical cord on T2-weighted imaging (Fig. 1C). Magnetic resonance spectroscopy (MRS) showed decreased N-acetylaspartate and increased choline and myo-inositol in the brainstem (Fig. 1D). These imaging findings were suggestive juvenile type of AxD.

3. Methods

3.1. DNA isolation and sequencing

Genomic DNA was extracted from peripheral white blood cells using a QuickGene DNA Whole Blood Kit S (Fujifilm, Tokyo, Japan) according to the manufacturer's instructions. A PCR of all exons and exon–intron boundaries of the GFAP gene (NM_002055.4) was performed with specific primers using an Ex Taq PCR Version 1.0 Kit (Takara, Shiga, Japan) according to the manufacturer's instructions (Supplemental Table 1). The PCR fragments were sequenced using a BigDye Terminator Cycle Sequence Kit (v1.1; Applied Biosystems, Foster City, CA, USA). The patient and her family provided their written informed consent for the performance of genetic testing, which was approved by the ethics committee of Kanagawa Children's Medical Center.

3.2. Plasmids

The wild-type GFAP plasmid tagged with Turbo green fluorescent protein (GFP) at C-terminal end was utilized as an expression vector (pCMV6-AC-GFP; Origene Technologies, RG204548, Rockville, MD). Mutations of R416W, R258C, R239C were introduced by site directed mutagene is using a PrimeSTAR® Mutagenesis Basal kit (Takara, Shiga, Japan). The entire sequences of the mutated fragment were confirmed by direct sequencing.

3.3. Immunofluorescence

HeLa and U2-OS cells were plated at 2×10^4 cells per well in an 8 well chamber slide (0.8 cm^2 per well; Thermo Fisher Scientific, Inc., Waltham, MA). Cells were transfected with each plasmids (DNA; 400 μg per well) using Lipofectamine™-3000 (Invitrogen, Life Technologies, Carlsbad, USA) for 30 h. After transfection, the cells were washed twice with PBS and fixed with 4% paraformaldehyde for 20 min. After 3 washes with PBS for 5 min, the fixed cells were stained with Hoechst 33342 for 20 min at 37 °C. Coverslips were mounted onto slides with 0.2% DABCO (Sigma, St Louis, MO). Cells were visualized using a FluoView™ FV1000 confocal microscope (Olympus, Tokyo, Japan).

3.4. Automated High-throughput image acquisition and analysis

HeLa and U2-OS cells were transfected with the wild and mutant types of the GFAP plasmid in 96-well

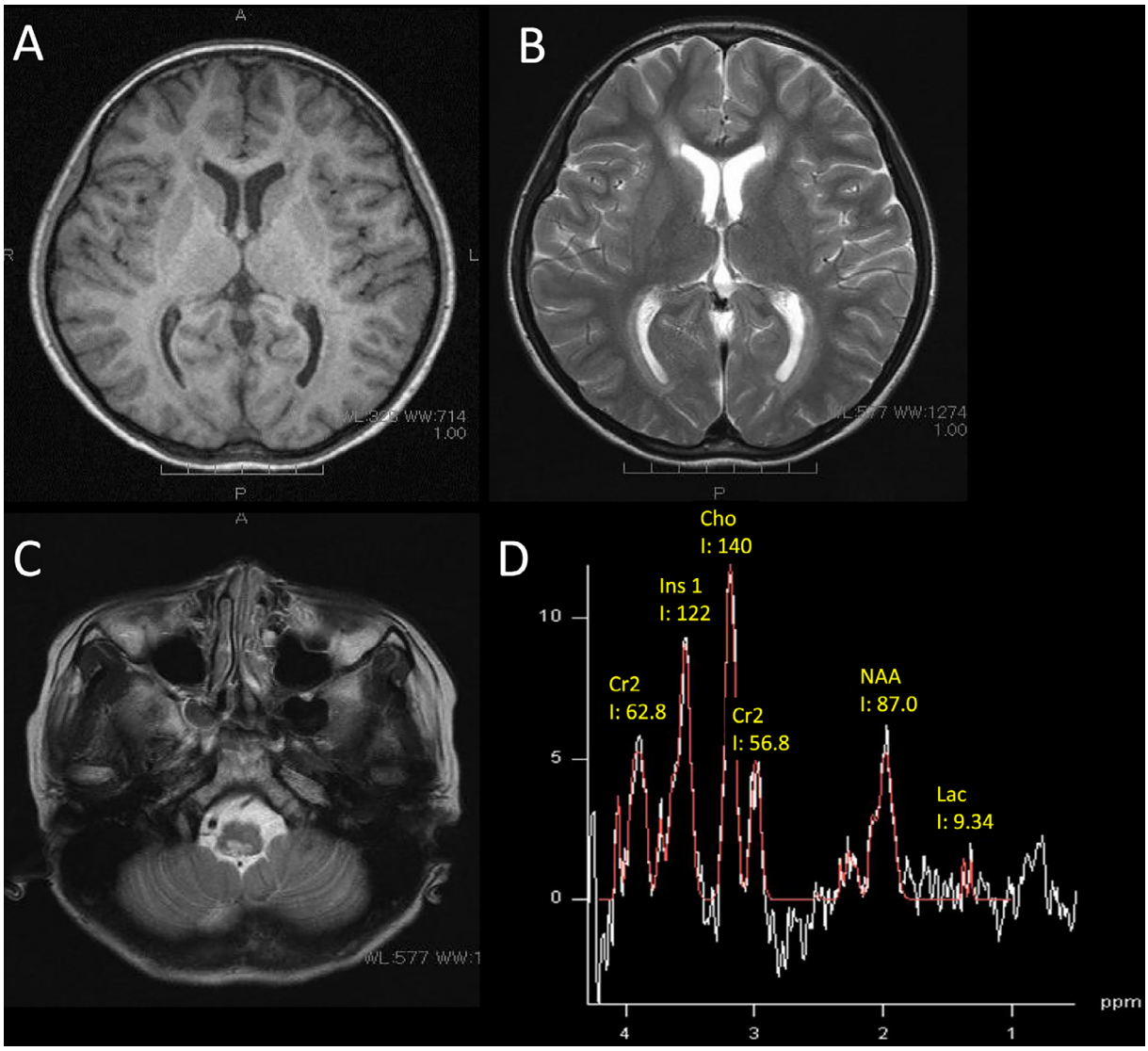

Fig. 1. Cranial MRI findings: Brain magnetic resonance imaging (MRI) revealed an area of high signal intensity along both of the lateral ventricles on T1-weighted imaging (A) and an area of decreased signal intensity on the periventricular rim that was surrounded by a region of high signal intensity on T2-weighted imaging (B). High signal intensity was observed from the lower medulla oblongata to the upper cervical cord on T2-weighted imaging (C). Magnetic resonance spectroscopy (MRS) showed decreased N-acetylasparate (NAA) and increased choline (Cho) and myo-inositol in the brainstem (D).

plates. After transfection, cells were washed twice with PBS and stained with Hoechst 33342 for 20 min at 37 °C. Then, they were fixed with 4% paraformaldehyde for 20 min at RT. An In Cell Analyzer 1000 (GE Healthcare, Little Chalfont, UK) was used for the automated detection of aggregates. This instrument generates fluorescence microscopy images of cell samples from a multi-well plate format in an automated manner, then performs an automated image analysis. Five images per well were acquired with a 20 × objective and a numerical aperture of 0.45. The nucleus of each cell was detected by a blue DAPI filter (xenon lamp, excitation at 360 nm and emission at 460 nm). GFP-GFAP were detected using a green GFP filter (excitation at 480 nm, emission at 535 nm), and the cell shape was detected on a bright field image. Images were analyzed using the In cell Developer software program (GE Healthcare). GFP-GFAP aggregate-positive cells were defined as cells possessing aggregates of 1–10 μm in size. The percentages of GFP-GFAP expressing cells with aggregation (1–10 μm) were calculated. We repeated this experiment 5 times. The data are expressed as the mean ± standard error of the mean. Student's *t*-test was used for comparisons between 2 groups. P values of <0.05 were considered to indicate statistical significance.

The study protocol of this study is approved by the Ethical Committee of Jichi Medical University.

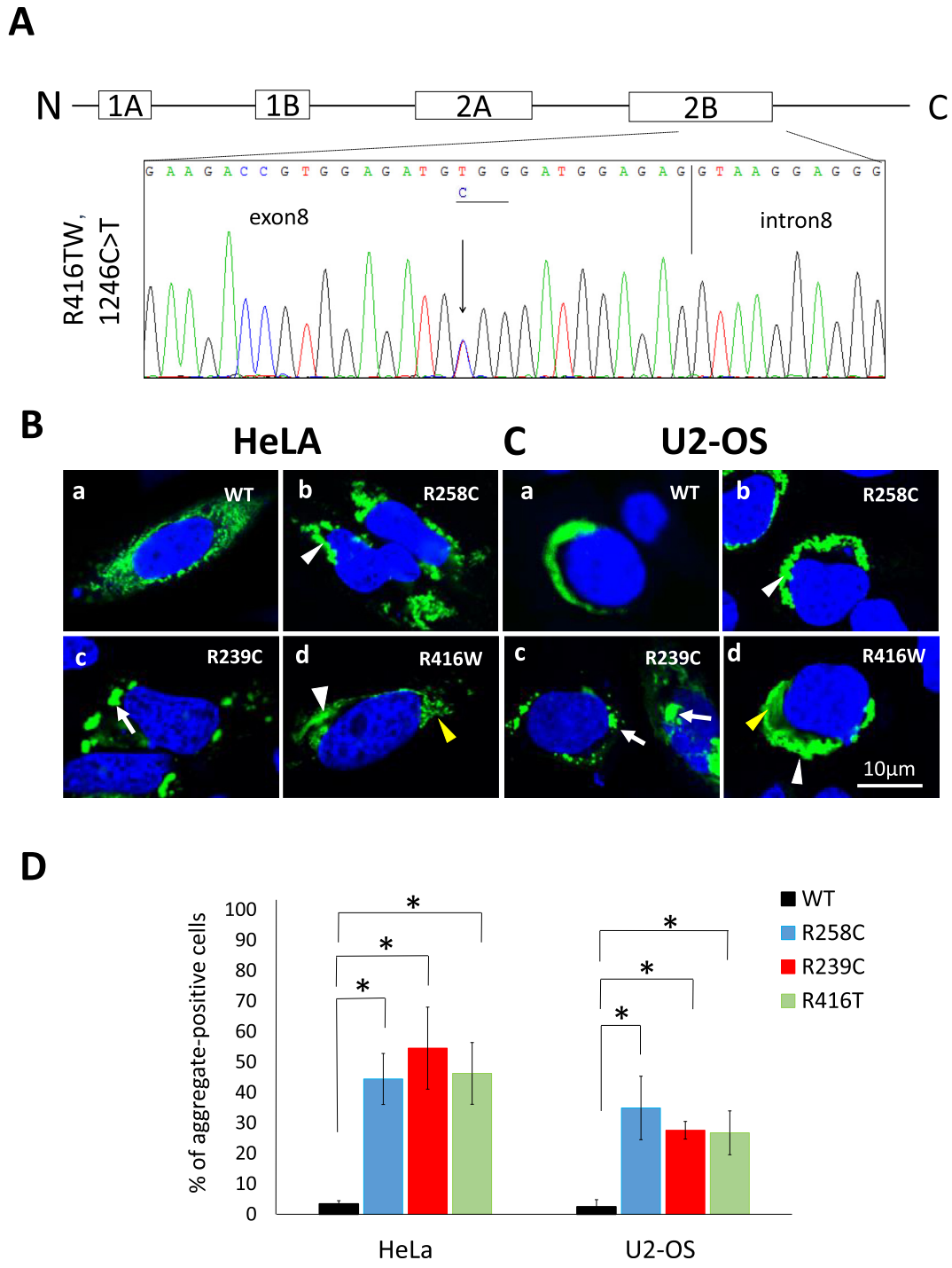

Fig. 2. Panel A: Direct sequencing of GFAP. Arrows indicate mutation c.1246C > T (p.R 416 W) in exon 8 of helical domain 2A. This mutation was not detected in parents (data not shown). 1A, 1B, 2A, 2B; helical domains of GFAP. Panels B and C: HeLa (Panel B) and U2-OS (Panel C) cells were transfected with $GFAP^{WT}$ (a) and the mutant plasmids (b; $GFAP^{R416W}$, c; $GFAP^{R258C}$, d; $GFAP^{R239C}$). Images were obtained by confocal microscopy. The localization of GFAP-GFP was detected. The nuclei were stained with Hoechst 33342 (blue). $GFAP^{WT}$ showed fine mesh like structures (a; Panels B and C). $GFAP^{R258C}$ showed bead-like fibrous aggregates of irregular thickness (white arrowheads) (b; Panels B and C). $GFAP^{R239C}$ showed large aggregates (>2 µm) (arrows) (c; Panels B and C). $GFAP^{R416W}$ showed both bead-like fibrous aggregates of irregular thickness (white arrowheads) and the fine dot pattern found in the wild-type (yellow arrowheads) (d; Panels B and C). Scale bars, 10 µm. Panel D: The comparison of the percentage of aggregate-positive cells in WT and mutant-derived U2-OS and HeLa cell lines as measured by an In Cell Analyzer 1000. An increase in aggregation was seen in mutants ($GFAP^{R416W}$, $GFAP^{R258C}$, *and* $GFAP^{R239C}$) in both the HeLa and U2-OS cell lines. The differences in comparison to WT were significant ($^{*}P < 0.05$ by Student's *t*-test) (D).

4. Results

4.1. DNA sequencing

Sanger sequencing identified a recurrent *de novo* heterozygous one base substitution in *GFAP*, c.1246C>T (p.R416W) in helical domain 2A (Fig. 2A) [1,8,10]. We investigated the consequences of this mutation by comparing the *in vitro* transient expression of mutant protein to that observed with other mutations (the mild type of c.772C>T (p.R258C), and the severe type of c.715C>T (p.R239C) [1].

4.2. Confocal immunofluorescence microscopy

The intracellular localization of wild-type $GFAP^{WT}$, and mutants ($GFAP^{R416W}$, $GFAP^{R258C}$, $GFAP^{R239C}$). GFAP was examined by confocal microscopy. In the majority of cells, $GFAP^{WT}$ exhibited a mesh like expression throughout the cytoplasm in both HeLa and U2-OS cells, similar to the expression observed in previous studies (a, Panels B,C; Fig. 2) [11,12]. The mild type mutant $GFAP^{R258C}$ showed a bead-like thick filamentous pattern composed of small aggregates (~1–2 μm) in both HeLa and U2-OS cells (b, Panels B,C; Fig. 2). Severe type mutant $GFAP^{R239C}$ showed large, distinct, aggregates (>2 μm) in the cytoplasm in both cell lines (c, Panels B,C; Fig. 2). $GFAP^{R416W}$ and showed a mixture of thick filamentous and small dot staining patterns that shared the features of both wild-type and mild type mutants (d, Panels B,C; Fig. 2).

4.3. Quantitative image analysis

We used an In Cell Analyzer to quantitatively count GFAP aggregation in live images [13]. After transfection in both HeLa and U2-OS cell lines, we quantitatively counted the cells containing aggregates, which were defined as circular green-stained areas of 1–10 μm in size (Fig. 2D). This analysis revealed that the number of aggregate-positive cells in the mutants ($GFAP^{R416W}$, $GFAP^{R258C}$, $GFAP^{R239C}$) was significantly increased in comparison to the WT control ($^{*}P < 0.05$, Fig. 2D). We could not find significant differences between the mutants.

5. Discussion

We reported the case of a patient with mild AxD with a c.1246C>T (p.R416W) mutation in *GFAP*. This mutation has already been reported in nine mild and two severe cases of AxD [1,7,8]. The biochemical character of GFAP with p.R416W has been studied in adrenal cortex carcinoma SW/cl.1, SW13/cl.2, and astrocyte U343MG cell lines [11,12]. Both studies qualitatively showed the aggregate formation by this mutation [11,12]. Recently, it was reported in a patient with adult-onset AxD and a non-symptomatic carrier [9]. Thus, to prove the pathogenicity of this mutation, we examined the aggregate formation of $GFAP^{R416W}$ in different cell lines and quantitatively analyzed aggregate formation using an In Cell Analyzer.

Firstly, we compared the expression pattern of this mutant with the wild-type and $GFAP^{R258C}$, $GFAP^{R239C}$ mutants found in AxD. $GFAP^{R416W}$ showed cellular localization and aggregate formation that are partially similar to both mild type and wild type of GFAP. This study suggest the modest tendency of aggregate formation by R416W mutation and may explain the mild clinical phenotype of the patient.

Secondary, we quantified the aggregate formation of $GFAP^{R416W}$ together with other mutations using an In Cell Analyzer, which quantitatively proved a significant increase in aggregates in cells that transiently expressed $GFAP^{R416W}$ as well as other mutants. In Cell Analyzer has been utilized for various types of quantitative analyses [13]. To the best of our knowledge, it has been never applied in the analysis of aggregate formation by GFAP. There is no effective drug therapies for AxD. This method, quantitatively detecting aggregate formation, seems feasible for drug screening of AxD.

In conclusion, we reported a mild type AxD patient with p.R416W in *GFAP* with precocious puberty. We firstly utilized In Cell analyzer to prove the tendency of aggregate formation by *GFAP* mutation. In Cell analyzer would be a valuable tool to prove the functional consequence by *GFAP* mutation and screen drug that decrease aggregate formation, which is hallmark for AxD.

Acknowledgments

This work was supported by a project grant for Health Research on Infants, Children, Adolescents, and Young Adults, from the Agency of Medical Research and Development to YT and was also supported by JSPS KAKENHI Grant Number 15552768 for HO.

Appendix A. Supplementary data

Supplementary data associated with this article can be found, in the online version, at https://doi.org/10.1016/j.braindev.2018.08.009.

References

[1] Srivastava S, Naidu S. Alexander disease. In: Pagon RA, Adam MP, Ardinger HH, Wallace SE, Amemiya A, Bean LJH, et al, editors. GeneReviews. Seattle, WA: All rights reserved; 1993.

[2] Johnson AB. Alexander disease: a review and the gene. Int J Dev Neurosci 2002;20:391–4.
[3] Coelho-Aguiar Jde M, Bon-Frauches AC, Gomes AL, Verissimo CP, Aguiar DP, Matias D, et al. The enteric glia: identity and functions. Glia 2015;63:921–35.
[4] Kondo T, Funayama M, Miyake M, Tsukita K, Era T, Osaka H, et al. Modeling Alexander disease with patient iPSCs reveals cellular and molecular pathology of astrocytes. Acta Neuropathol Commun 2016;4:69.
[5] Prust M, Wang J, Morizono H, Messing A, Brenner M, Gordon E, et al. GFAP mutations, age at onset, and clinical subtypes in Alexander disease. Neurology 2011;77:1287–94.
[6] Li R, Messing A, Goldman JE, Brenner M. GFAP mutations in Alexander disease. Int J Dev Neurosci 2002;20:259–68.
[7] Pareyson D, Fancellu R, Mariotti C, Romano S, Salmaggi A, Carella F, et al. Adult-onset Alexander disease: a series of eleven unrelated cases with review of the literature. Brain 2008;131:2321–31.
[8] Brenner M, Johnson AB, Boespflug-Tanguy O, Rodriguez D, Goldman JE, Messing A. Mutations in GFAP, encoding glial fibrillary acidic protein, are associated with Alexander disease. Nat Genet 2001;27:117–20.
[9] Liu Y, Zhou H, Wang H, Gong X, Zhou A, Zhao L, et al. Atypical MRI features in familial adult onset Alexander disease: case report. BMC Neurol 2016;16:211.
[10] van der Knaap MS, Ramesh V, Schiffmann R, Blaser S, Kyllerman M, Gholkar A, et al. Alexander disease: ventricular garlands and abnormalities of the medulla and spinal cord. Neurology 2006;66:494–8.
[11] Der Perng M, Su M, Wen SF, Li R, Gibbon T, Prescott AR, et al. The Alexander disease-causing glial fibrillary acidic protein mutant, R416W, accumulates into Rosenthal fibers by a pathway that involves filament aggregation and the association of alpha B-crystallin and HSP27. Am J Hum Genet 2006;79:197–213.
[12] Yoshida T, Nakagawa M. Clinical aspects and pathology of Alexander disease, and morphological and functional alteration of astrocytes induced by GFAP mutation. Neuropathology 2012;32:440–6.
[13] Pfisterer SG, Mauthe M, Codogno P, Proikas-Cezanne T. Ca2+/calmodulin-dependent kinase (CaMK) signaling via CaMKI and AMP-activated protein kinase contributes to the regulation of WIPI-1 at the onset of autophagy. Mol Pharmacol 2011;80:1066–75.